First-principles investigations of the pressure-induced structural transitions in $Mg(AlH_4)_2$

2007 J. Phys.: Condens. Matter 19 176205

(http://iopscience.iop.org/0953-8984/19/17/176205)

IOP PUBLISHING JOURNAL OF PHYSICS: CONDENSED MATTER

J. Phys.: Condens. Matter **19** (2007) 176205 (11pp) doi:10.1088/0953-8984/19/17/176205

First-principles investigations of the pressure-induced structural transitions in $Mg(AlH_4)_2$

C H Hu[1], D M Chen[1], Y M Wang[2,4], D S Xu[3] and K Yang[1]

[1] National Engineering Research Center, Institute of Metal Research, Chinese Academy of Sciences, 72 Wenhua road, Shenyang 110016, People's Republic of China
[2] Shenyang National Laboratory for Materials Science, Institute of Metal Research, Chinese Academy of Sciences, 72 Wenhua road, Shenyang 110016, People's Republic of China
[3] Titanium Alloys Laboratory, Institute of Metal Research, Chinese Academy of Sciences, 72 Wenhua road, Shenyang 110016, People's Republic of China

E-mail: ymwang@imr.ac.cn

Received 20 September 2006, in final form 1 March 2007
Published 28 March 2007
Online at stacks.iop.org/JPhysCM/19/176205

Abstract

A systematic investigation is presented of the high-pressure structural stability of $Mg(AlH_4)_2$ using a plane-wave pseudo-potential method. The total-energy calculations show that under ambient pressure the structure of α-$Mg(AlH_4)_2$ found by experiments is more stable than the other proposed structures, and with pressure increasing the α to β (δ-$Zr(MoO_4)_2$-type structure) and β to γ ($Ca(BF_4)_2$-type structure) transitions occur at 0.67 and 10.28 GPa respectively, accompanied with volume reductions of 6.6% and 8.7%. A detailed study of the electronic structures reveals the bonding characteristics between Al and H and between Mg and H as well as the nonmetallic features of α, β, and γ phases under pressure of up to 20.0 GPa. Their electronic structures are mainly responsible for the relative high-pressure stability of the three phases. Finally, an analysis of their structural relations indicates that it is possible to produce the $\alpha \rightarrow \beta \rightarrow \gamma$ structural transition by applying pressure.

(Some figures in this article are in colour only in the electronic version)

1. Introduction

There has been laborious effort made to explore sustainable hydrogen storage materials for mobile applications. A good hydrogen storage material should have synchronously a high gravimetric hydrogen density (GHD) and the ability of safe, fast and fully reversible hydrogenation under ambient conditions. Conventional metal hydrides such as $LaNi_5$, FeTi, and $Ti_{1.2}Mn_{1.8}$ seem not to satisfy these requirements due to their intrinsic low GHD (in

[4] Author to whom any correspondence should be addressed.

general, <2.5 wt%) [1], although they present a good cycling performance under moderate conditions. Now complex hydrides, $A_x(MH_4)_y$ (A = Li, Na, K, Mg, Ca, Sr; M = B or Al), with very high GHD (for example, 7.5 wt% H in $NaAlH_4$), are generally thought to be a promising class of hydrogen storage materials [2–9]. However, an open question is raised about how to improve their kinetics of absorbing/desorbing hydrogen. Since Bogdanovic and Schwickardi [2] have found that $NaAlH_4$ with transition metal catalysts can rapidly release 5.6 wt% H under moderate conditions, the door for employing these complex hydrides as reversible hydrogen materials appears to be opened. Subsequently, many experimental and theoretical studies on these systems have followed in turn.

Recently, the magnesium alanate $Mg(AlH_4)_2$, one of the alkali earth alanates, has attracted scientific interest due to its higher theoretical hydrogen capacity (9.3 wt%) than that of $NaAlH_4$, expected to be another potential material for hydrogen storage. Its crystal structure (hereafter, α-$Mg(AlH_4)_2$) has been determined by recent x-ray and neutron diffraction experiments [10, 11]. The electronic structure and vibrational properties of some magnesium alanates have been calculated by Setten *et al* [12], Spanò and Bernasconi [13], respectively, using *ab initio* methods. However, to our best knowledge, a systematic high-pressure study on $Mg(AlH_4)_2$ has not been reported yet. Furthermore, so far as properties of materials closely related their crystalline structures are concerned, it is difficult to describe them only by experiments without the help of theoretical calculations, especially for these materials containing atoms with a low atomic number, for instance, hydrogen atoms, due to their poor scattering ability to x-photons, electrons and neutrons. The main aim of the present work is just to study the structural transition of $Mg(AlH_4)_2$ under high-pressure conditions using a first-principles total-energy calculation.

Recently, first-principles methods have been successfully applied to predict the pressure-induced structural transitions of various materials from simple metals to complex compounds such as Ti [14], MgH_2 [15], $LiAlH_4$ [16], $NaAlH_4$ [17], $NaBH_4$ [18], for which their phase transitions have been reproduced by high-pressure experiments [18–21]. Their success encourages us to investigate systematically the electronic structure and the pressure-induced structural transition of $Mg(AlH_4)_2$. Seven closely related potential structures have been considered in our present work. They are namely α-$Mg(AlH_4)_2$ (trigonal; $P\bar{3}m1$) [11], α-$Zr(MoO_4)_2$ (trigonal; $P\bar{3}1c$) [22], δ-$Zr(MoO_4)_2$ (monoclinic; $C2/m$) [22], $Ca(BF_4)_2$ (orthorhombic; $Pbca$) [23], $Zr(WO_4)_2$ (cubic; $P2_13$) [24], $Mg(AlCl_4)_2$ (monoclinic; $C2/c$) [25], and $Cu(AlCl_4)_2$ (triclinic; $P\bar{1}$) [26].

2. Computational details

All the electronic-structure calculations in this work were performed using the CASTEP code [27]. It is based on density-functional theory (DFT) with a plane-wave ultrasoft pseudo-potential (PW-USPP) method [28]. The generalized gradient approximation (GGA) of Perdew and Wang [29] was used to describe the exchange–correlation functional. To obtain the accurate minimum total energy for a particular structural arrangement, all ions in the computational cells were allowed full relaxation to all the volumes considered in the present calculations using the BFGS minimization algorithm [30]. The Pulay density mixing scheme [31] was used to generate a new starting charge density during the self-consistent field (SCF) total-energy calculation. The SCF calculation was considered to have converged when the energy change was lower than our predefined value 10^{-6} eV/atom. In order to decrease the error resulting from the choice of plane-wave basis sets and k-points, the cut-off energy was set to 360 eV and the k-point spacing, smaller than 0.04 $Å^{-1}$, was individually adjusted in reciprocal space, not

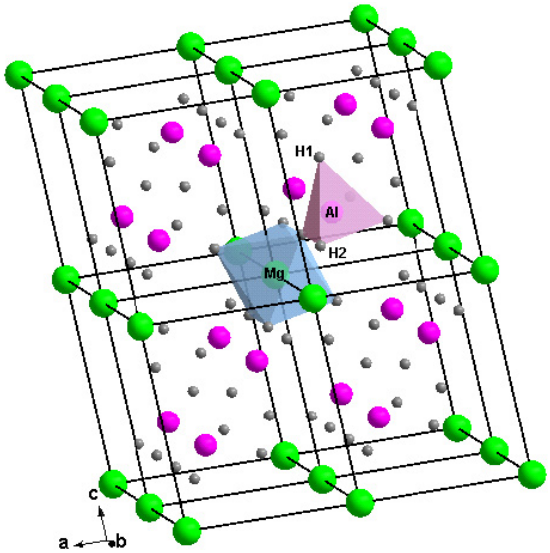

Figure 1. $2 \times 2 \times 2$ cell of α-$Mg(AlH_4)_2$ with space group $P\bar{3}m1$. The tetrahedron and octahedron in it represent AlH_4 and MgH_6 complexes, respectively.

only to the size of each computational cell of the nine crystallographic structures of $Mg(AlH_4)_2$ given below, but also to its variation at a given compressed volume.

3. Results and discussion

3.1. Structural properties of $Mg(AlH_4)_2$

As mentioned above, the recent x-ray powder-diffraction experiments have confirmed that, under ambient conditions, the structure of α-$Mg(AlH_4)_2$ shown in figure 1 has the space-group symmetry $P\bar{3}m1$ with a CdI_2-layered structure. In fact, in α-$Mg(AlH_4)_2$ and other proposed magnesium alanates, except for the $Ca(BF_4)_2$-type structure in which magnesium atom located at the centre of a distorted square anti-prism is coordinated by eight H atoms, there almost exist two kinds of polyhedra: one is the AlH_4 tetrahedron in which the aluminium atom is tetrahedrally coordinated by one H_1 and three H_2 atoms, and the other is the MgH_6 octahedron in which the magnesium atom is octahedrally coordinated by six H_2 atoms.

The calculated total-energy versus volume (E–V) curves respectively for one formula unit (f.u.) of α-$Mg(AlH_4)_2$ and other proposed crystallographic structures of magnesium alanates are fitted using the universal equation of state (U-EOS) [32] and shown in figure 2. It demonstrates that under ambient conditions, the structure of α-$Mg(AlH_4)_2$ may be more stable than other structures considered in the present study. For example, at their equilibrium volumes the calculated total energy for α-$Mg(AlH_4)_2$ is 107.1 and 203.8 meV/f.u. lower than the corresponding values for the $Zr(WO_4)_2$-type and $Ca(BF_4)_2$-type structures, respectively. However, it is found from this figure that the total-energy differences of α-$Mg(AlH_4)_2$ from α- and δ-$Zr(MoO_4)_2$-type at these volumes are only 7.7 and 25.5 meV/f.u., respectively. These results imply that the stability of these magnesium alanates is more sensitive to the change in their volumes caused by pressure, temperature, and other thermodynamic conditions, namely, it is easier for their structures to undergo a phase transition with each

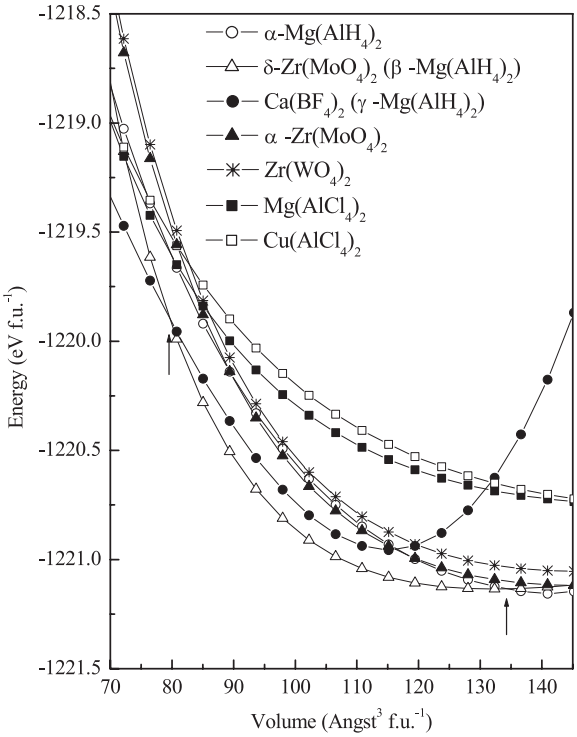

Figure 2. Total energy (in eV/f.u.) versus atomic volume (in $Å^3$/f.u.) curves for α-$Mg(AlH_4)_2$ and other proposed structures of magnesium alanates as denoted on top in this figure. The $\alpha \rightarrow \beta$ and $\beta \rightarrow \gamma$ structural transition points are marked by two arrows, respectively.

other. Figure 2 shows that in all E–V curves for the magnesium alanates considered in our study, the curves for α-$Mg(AlH_4)_2$ and δ-$Zr(MoO_4)_2$ structures (hereafter β-$Mg(AlH_4)_2$) first intersect once the volume is smaller than 134.3 $Å^3$, and then the curve for β-$Mg(AlH_4)_2$ will intersect with that for the $Ca(BF_4)_2$-type structure (hereafter γ-$Mg(AlH_4)_2$) once the volume is reduced to 80.5 $Å^3$. This result indicates that with their volumes compressed continuously, a series of structural transitions will appear as the following sequence: α-$Mg(AlH_4)_2 \rightarrow \beta$-$Mg(AlH_4)_2 \rightarrow \gamma$-$Mg(AlH_4)_2$ ($\alpha \rightarrow \beta \rightarrow \gamma$). To give evidence of the reliability of such a theoretical predication we calculated the optimized lattice parameters, internal parameters and bulk modules of α-, β- and γ-$Mg(AlH_4)_2$ and list them in table 1. In this table the deviation of the lattice constants and internal parameters calculated by us from the experimental [10, 11] and theoretical predictable values [12, 13] for α-$Mg(AlH_4)_2$ is within 2%, which is sufficiently accurate. In addition, these values for γ-$Mg(AlH_4)_2$ are also comparable with the calculated ones for $Ca(AlH_4)_2$ from [33]. The calculated bulk moduli B_0 in table 1 are 9.2, 6.8, and 34.7 GPa for α-, β-, and γ-$Mg(AlH_4)_2$, respectively; unfortunately there is no experimental evidence to prove them, to our best knowledge. At first glance, the bulk modulus of γ-$Mg(AlH_4)_2$ is about four times as large as that of α-$Mg(AlH_4)_2$, the hardest one among the three phases, but it is still very easily compressible compared with classical hydrides; for example, the values of B_0 are 51.0, 135.3, and 140.0 GPa for MgH_2 [15], TiH_2 [34], and $LaNi_5H_7$ [35], respectively.

Table 1. Calculated structural parameters of α-$Mg(AlH_4)_2$, β-$Mg(AlH_4)_2$ (δ-$Zr(MoO_4)_2$ type), and γ-$Mg(AlH_4)_2$ (($CaBF_4)_2$ type). For comparison, the corresponding experimental values of α-$Mg(AlH_4)_2$ are also given in the following parentheses.

Structure	Lattice constants (Å)	Internal parameters	B_0 (GPa)
α-$Mg(AlH_4)_2$	$a = 5.201$ (*5.208*)	Mg: 0.0000, 0.0000, 0.0000 (*0.0000, 0.0000, 0.0000*)	9.2
($P\bar{3}m1$)	$c = 5.960$ (*5.839*)	Al: 0.3333, 0.6667, 0.7030 (*0.3333, 0.6667, 0.6991*)	
		H1: 0.3333, 0.6667, 0.4364 (*0.3333, 0.6667, 0.4242*)	
		H2: 0.1682, −0.1682, 0.8074 (*0.1671*, *−0.1671, 0.8105*)	
β-$Mg(AlH_4)_2$	$a = 9.027$	Mg: 0.0000, 0.0000, 0.0000	6.8
(δ-$Zr(MoO_4)_2$: $C2/m$)	$b = 5.194$	Al: 0.3273, 0.0000, 0.2908	
	$c = 6.073$	H1: 0.0941, −0.2548, 0.8207	
	$\beta = 89.55$	H2: 0.1601, 0.0000, 0.2036	
		H3: 0.3341, 0.0000, 0.5496	
γ-$Mg(AlH_4)_2$	$a = 12.722$	Mg: 0.1126, −0.4807, 0.2032	34.7
($Ca(BF_4)_2$ type: $Pbca$)	$b = 8.827$	Al1:−0.0557, −0.2275, 0.0248	
	$c = 8.588$	Al2: 0.1509, −0.1251, 0.3015	
		H1: −0.0148, −0.3593, 0.1417	
		H2: 0.1383, 0.3860, 0.3892	
		H3: 0.1292, 0.3217, 0.0972	
		H4: 0.0375, −0.3558, 0.4325	
		H5: 0.1584, −0.0938, 0.4856	
		H6: 0.0298, −0.1028, 0.2416	
		H7: 0.1878, −0.2944, 0.2599	
		H8: 0.2238, −0.0082, 0.2057	

3.2. High-pressure behaviour of $Mg(AlH_4)_2$

By comparing the Gibbs free energies (G) of the α-, β- and γ-$Mg(AlH_4)_2$, it can be determined when a structural transition starts. In the case of the calculation being performed at absolute zero, $G = E + PV - TS$ becomes the enthalpy $H = E + PV$. Therefore, only the relative enthalpy ($= H - E_{\alpha-Mg(AlH_4)_2}$) versus pressure ($H$–$P$) curves are calculated and plotted in the inset of figure 3. In this figure, H is more negative for the β phase than for the α phase; that is, the β phase is more stable than the α phase once the external pressure P is beyond 0.67 GPa. For the same reason, the γ phase is also more stable than the β phase once P is beyond 10.28 GPa. From this figure, the transition pressures for the $\alpha \rightarrow \beta$ and $\beta \rightarrow \gamma$ transitions are determined to be 0.67 and 10.28 GPa, respectively.

In addition, from the calculated pressure versus volume (P–V) curves for α-, β- and γ-$Mg(AlH_4)_2$ in figure 3, it can be found that the corresponding volume contractions at these structural transition points are about 6.6% and 8.7%, respectively. Although such contractions are still not verified by experiments, they may not be unbelievable in terms of the following considerations. First, they are comparable to the 17% and 4% volume contractions calculated in the $\alpha \rightarrow \beta$ transition for $LiAlH_4$ [16] and $NaAlH_4$ [17]. Second, some high-pressure x-ray powder diffraction experiments [36, 37] have indeed found a large volume collapse at the structural transition points.

3.3. Electronic structures of $Mg(AlH_4)_2$

To detail the variation in the electronic structures that are correlated with these structural transitions, the electronic density of states (DOS) and partial DOS (PDOS) for α- (at equilibrium), β- (at transition point; 0.67 GPa), and γ-$Mg(AlH_4)_2$ (at the transition point;

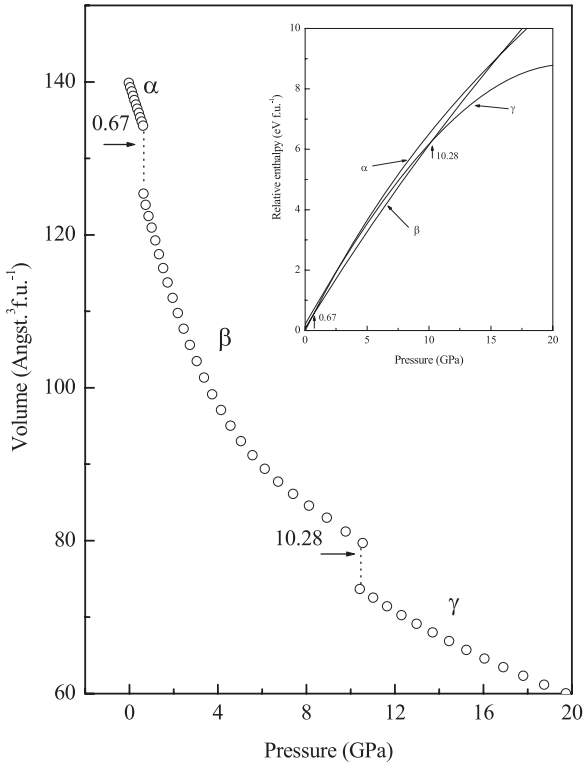

Figure 3. Volume (in f.u.) versus pressure curves for α-, β-, and γ-$Mg(AlH_4)_2$. The relative enthalpy curves of the α-, β-, and γ-$Mg(AlH_4)_2$ as a function of pressure are shown in the inset.

10.28 GPa) have been calculated, and they are presented in figure 4. The common characteristics in the electronic structures can be drawn from this figure. First, they exhibit a nonmetallic behaviour characterized by a energy band gap (E_g) between the valence band (VB) and the conduction band (CB), even at pressures up to 20.0 GPa, like $NaAlH_4$ [17], $NaBH_4$ [18], $Ca(AlH_4)_2$ [33]. Second, the VB is mainly dominated by H 1s, and Al s, p states, and the contribution of Mg s, p states to it is negligible. In the total DOS for α- and β-$Mg(AlH_4)_2$, the VB is split into two separate peaks. In addition, the Al s, p and H s states are energetically degenerate in the VB region, which clearly facilitates the H–Al hybridization and the formation of directionally covalently bonded AlH_4 tetrahedron subunits in them. The Mg s, p states are mainly distributed in the CB above the energy region of the Fermi energy level, E_f, and exhibit an anti-bonding interaction with H 1s states, which is consistent with the ionic bonding between Mg and the AlH_4 subunit. Furthermore, the calculated DOS for α-$Mg(AlH_4)_2$ is also in a good agreement with the recent theoretical results given by Setten *et al* [12].

The difference of the DOS between α- and β-$Mg(AlH_4)_2$ is not very obvious, other than the broader CB for β- than for α-$Mg(AlH_4)_2$. However, on going through the $\beta \rightarrow \gamma$ structural transition, the DOS of β-$Mg(AlH_4)_2$ is markedly changed from that of γ-$Mg(AlH_4)_2$. In the DOS for γ-$Mg(AlH_4)_2$, there can be found more mixing of the s and p states for Al, which may mirror the increase in the hybridization between them. This increase comes from the modification of the H environment of Al from tetrahedral in the β phase to deformed octahedral in the γ phase. Moreover, we can deduce the weakening of the anti-bonding interaction

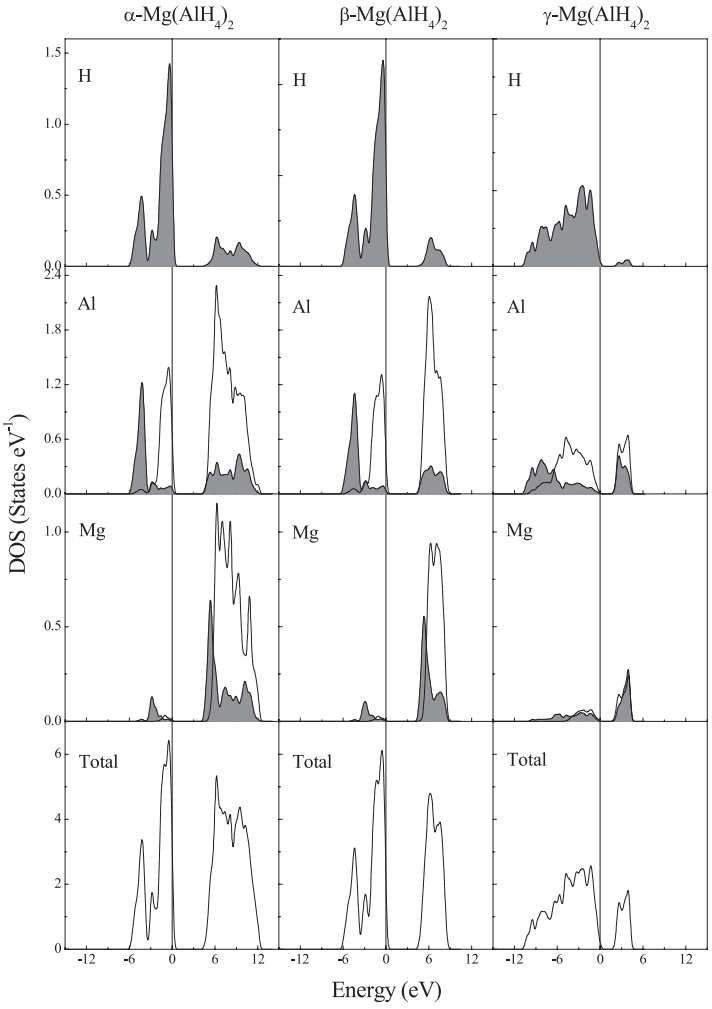

Figure 4. Calculated total and partial electronic densities of states (DOSs) for α- (at equilibrium), β- (at transition pressure; 0.67 GPa), and γ-$Mg(AlH_4)_2$ (at transition pressure; 10.28 GPa). The Fermi level is set to zero and marked in vertical lines. The s states in the PDOS are depicted as shaded-grey curves.

between Mg s, p and H s due to the $\alpha \rightarrow \beta \rightarrow \gamma$ transition from the PDOS reduction of Mg s, p and H s in the CB region. In this transition, the metallic character of $Mg(AlH_4)_2$ will become more and more obvious, which can be reflected from the reduction in E_g ($E_g = 3.72$ for α-; > 3.67 for β-; and > 1.21 eV for γ-$Mg(AlH_4)_2$).

To understand quantitatively the bonding interactions in $Mg(AlH_4)_2$, we calculated the average net charge (ANC) and bond overlap population (BOP) [38] on the basis of the Mulliken population [39], similar to our previous works [40, 41]. As mentioned in [38], by projecting the plane-wave eigenfunctions onto a linear combination of atomic orbital basis set, the bond overlap population (bond order) between two atoms A and B can be defined as $BOP_{A-B} = \sum_k (w_k) \sum_\mu^{onA} \sum_\nu^{onB} 2P_{\mu\nu}(k)S_{\mu\nu}(k)$, where w_k are the weights associated with the calculated k points in the Brillouin zone, and $P_{\mu\nu}(k)$ and $S_{\mu\nu}(k)$ are the density matrix and overlap matrix, respectively. In order to describe quantitatively the bonding characteristics in

Table 2. Calculated average net charge (ANC) of H1, H2, Al and Mg in α- (at equilibrium), β- (at transition pressure; 0.67 GPa), and γ-$Mg(AlH_4)_2$ (at transition pressure; 10.28 GPa).

	H1	H2	Al	Mg
α-$Mg(AlH_4)_2$ (0.0 GPa)	−0.34	−0.60	0.99	2.32
β-$Mg(AlH_4)_2$ (0.67 GPa)	−0.35	−0.60	0.98	2.37
γ-$Mg(AlH_4)_2$ (10.28 GPa)	−0.49[a]	—	0.78[a]	2.29[a]

[a] In γ-$Mg(AlH_4)_2$, Mg is located at the centre of a distorted square anti-prism and coordinated by eight H atoms, and the initial AlH_4 tetrahedron is transformed into a distorted AlH_6 octahedron accompanied by the $\beta \rightarrow \gamma$ structural transition.

Table 3. Average bond length (BL) and scaled bond overlap population (BOP^s) between Al and H1, between Al and H2 and between Mg and H2 in AlH_4 and MgH_6 polyhedra in α- (at equilibrium), β- (at transition pressure; 0.67 GPa), and γ-$Mg(AlH_4)_2$ (at transition pressure; 10.28 GPa).

	Al–H1		Al–H2		Mg–H2	
	BL	BOP^s	BL	BOP^s	BL	BOP^s
α-$Mg(AlH_4)_2$ (0.0 GPa)	1.576	0.603	1.602	0.443	1.909	−0.304
β-$Mg(AlH_4)_2$ (0.67 GPa)	1.574	0.604	1.596	0.464	1.885	−0.308
γ-$Mg(AlH_4)_2$ (10.28 GPa)	1.709[a]	0.412[a]	—	—	1.953[a]	−0.148[a]

[a] The notes are the same as those in table 2.

AlH_4 (or MgH_6) subunit in $Mg(AlH_4)_2$, the definition of the scaled BOP (BOP^s) in [40, 41] is kept, namely, $BOP^s_{Al(Mg)-H} = BOP_{Al(Mg)-H}/BL_{Al(Mg)-H}$, where $BL_{Al(Mg)-H}$ is the average bond length between Al(Mg) and H atoms. The positive and negative BOP^s values indicate bonding and anti-bonding states, respectively. The calculated ANC and BOP^s for α- (at equilibrium), β- (at transition pressure; 0.67 GPa), and γ-$Mg(AlH_4)_2$ (at transition pressure; 10.28 GPa) are listed in tables 2 and 3. It can be seen from table 2 that Mg is always a primary electron donor but that H is an electron acceptor, indicating that charges transfer mainly from Mg to the AlH_4 subunit. The BOP^s values in table 3 allow us to conclude that there are strong bonding interactions between H and Al atoms and anti-bonding interactions between H and Mg atoms. However, the BOP^s values for γ-$Mg(AlH_4)_2$ are very different from those for α- and β-$Mg(AlH_4)_2$, depending closely on the local H environments of Al and Mg in these magnesium alanates.

3.4. Structural relations of $Mg(AlH_4)_2$

Finally, we turn to investigate the structural relations and try to provide an insight into the mechanism of the structural transition of $\alpha \rightarrow \beta \rightarrow \gamma$-$Mg(AlH_4)_2$. In general, the bond compressibility along the three lattice axes is dissimilar in a crystal. However, in our case for the α-$Mg(AlH_4)_2$ to undergo a volume compression under a small pressure beyond 0.67 GPa, it can be expected that only a slight deformation would take place. In fact, the Al–H_1 and Al–H_2 bond lengths are shortened by only about 0.25% (from 1.576 to 1.572 Å) in α-$Mg(AlH_4)_2$ and by 0.56% (from 1.602 to 1.593 Å) in β-$Mg(AlH_4)_2$ at 0.67 GPa, and the characteristic tetrahedral AlH_4 subunit is maintained with a small tilt along the c axis. In this transition, the trigonal α-$Mg(AlH_4)_2$ is modified into the monoclinic β-$Mg(AlH_4)_2$. Such a structural modification is schematically illustrated in figure 5. As can be seen in this figure, the 9.009×5.201 Å two-dimensional rectangular cell in the $2 \times 2 \times 1$ supercell of α-$Mg(AlH_4)_2$ is transformed into a monoclinic two-dimensional unit cell of β-$Mg(AlH_4)_2$ with $a = 8.935$ Å, $b = 5.155$ Å, and $\beta = 89.32°$, only slightly deformed. In this case, the coordination numbers of H for Al and Mg

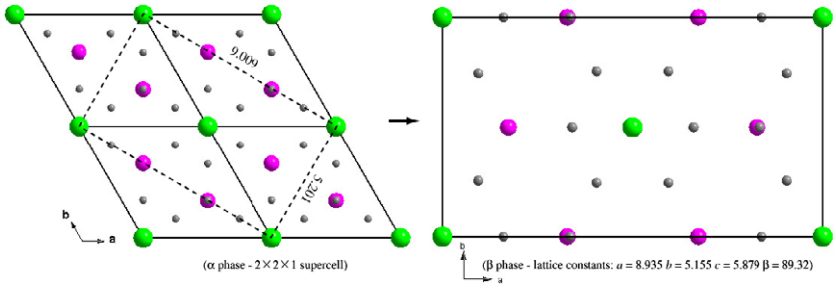

Figure 5. Illustration of the $\alpha \rightarrow \beta$ structural transition. Left and right figures represent the top-view of α- and β-$Mg(AlH_4)_2$ along the [001] direction, respectively. A 'monoclinic atomic array' of the β-$Mg(AlH_4)_2$ structure in $2 \times 2 \times 1$ cell of α-$Mg(AlH_4)_2$ is outlined by dotted lines.

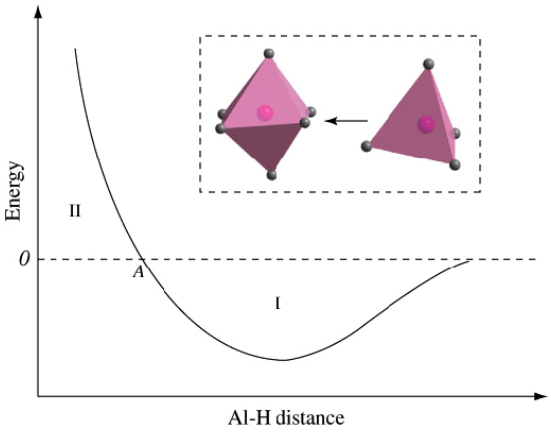

Figure 6. Schematic curve of Al–H bonding energy versus interatomic distance in AlH_4 and AlH_6 units for $Mg(AlH_4)_2$. The regions I and II marked in this figure represent the stabilizing and destabilizing range for Al–H bonding, respectively. Schematic AlH_4 and AlH_6 units are also depicted on top of this figure. The bonding energy between Al and H at infinite separation is set to zero.

are unchanged, from which it is quite understandable why the DOS for the β-$Mg(AlH_4)_2$ is so similar to that for α-$Mg(AlH_4)_2$ and the total-energy difference between α- and β-$Mg(AlH_4)_2$ at the ground state is so small. These results indicate that the $\alpha \rightarrow \beta$ transition would occur rapidly once the critical pressure is reached, which is called a *displacive transition*, as classified by Buerger [42]. However, the case for the β- to γ- $Mg(AlH_4)_2$ is different, since higher pressure would result in a drastic change not only in the β-$Mg(AlH_4)_2$ structure but also in the coordination numbers of H for Al and Mg. We can get some useful hints about the $\beta \rightarrow \gamma$ transition from the sketch of a typical Al–H binding energy curve shown in figure 6, in which the AlH_4 and AlH_6 units are schematically depicted. In a low range of pressure, the Al–H bond length in region I deviates just a bit from the equilibrium value and it will be able to return the minimum; namely, the AlH_4 unit is stable. With pressure further increasing, however, the bond length in region II deviates so much from its equilibrium value as hardly to keep AlH_4, since this would cost too much energy. The initial AlH_4-configuration would become unstable and be modified into the AlH_6-configuration, leading to the appearance of the $\beta \rightarrow \gamma$ transition. In fact, the previous work on the $\alpha \rightarrow \beta$ transition for $NaAlH_4$ [17] has predicted an increase in the coordination number of H for Al from 4 to 6. The $\beta \rightarrow \gamma$ transition process, called

a *reconstructive transition* [42], may be sluggish because it needs high activation energy to drive it.

4. Conclusions

In conclusion, a detailed study of the high-pressure structural transition in $Mg(AlH_4)_2$ has been performed using a first-principles total-energy calculation. The α-$Mg(AlH_4)_2$ found by experiments and another six closely related structures with different space groups have been considered in our present work. Our calculations show that α-$Mg(AlH_4)_2$ is more stable than the other proposed structures at the ground state and its optimized structural parameters are in good agreement with experimental data. With pressure increasing, the structural transitions from α- to β-$Mg(AlH_4)_2$ (δ-$Zr(MoO_4)_2$-type structure) and then to γ-$Mg(AlH_4)_2$($Ca(BF_4)_2$-type structure) occur at 0.67 and 10.28 GPa, accompanied with about 6.6% and 8.7% volume collapses, respectively. The change in the electronic structures and the variation in the average bond lengths between Al and H and between Mg and H in α-, β-, and γ-$Mg(AlH_4)_2$ have been discussed; it is found that they are responsible for such transitions under high pressures. Although all the α-, β-, and γ-$Mg(AlH_4)_2$ structures exhibit a common nonmetallic feature, their bonding characters between Al (or Mg) and H atoms are distinct. The mechanism of the high-pressure structural transition is described by analysing the variation in their structural and electronic structures. The $\alpha \rightarrow \beta \rightarrow \gamma$ transition under high pressure is believed to be feasible.

Acknowledgment

We acknowledge support through Grant No 10474102 from the National Natural Science Foundation of China.

References

[1] Sandrok G and Thomas G *IEA/DOE/SNL/Hydride Data Bases* (http://hydpark.ca.sandia.gov)
[2] Bogdanovic B and Schwickardi M 1997 *J. Alloys Compounds* **253/254** 1
[3] Zaluska A, Zaluski L and Ström-Olsen J O 2000 *J. Alloys Compounds* **298** 125
[4] Schlapbach L and Züttel A 2001 *Nature* **414** 353
[5] Gross K J, Majzoub E H and Spangler S W 2003 *J. Alloys Compounds* **356/357** 423
[6] Züttel A, Rentsch S, Fischer P, Wenger P, Sudan P, Mauron Ph and Emmenegger Ch 2003 *J. Alloys Compounds* **356/357** 515
[7] Renaudin G, Gomes S, Hagemann H, Keller L and Yvon K 2004 *J. Alloys Compounds* **375** 98
[8] Orimo S, Nakamori Y, Kitahara G, Miwa K, Ohba N, Towata S and Züttel A 2005 *J. Alloys Compounds* **404–406** 427
[9] Schwarz M, Haidue A, Stil H, Paulus P and Geerlings H 2005 *J. Alloys Compounds* **404–406** 762
[10] Fitchtner M, Engel J, Fuhr O, Glöss A, Rubner O and Ahlrichs R 2003 *Inorg. Chem.* **42** 7060
[11] Fossdal A, Brinks H W, Fichtner M and Hauback B C 2005 *J. Alloys Compounds* **387** 47
[12] van Setten M J, de Wijs G A, Popa V A and Brocks G 2005 *Phys. Rev.* B **72** 073107
[13] Spanò E and Bernasconi M 2005 *Phys. Rev.* B **71** 174301
[14] Ostanin S A and Trubitsin V Y 1997 *J. Phys.: Condens. Matter* **9** L491
[15] Vajeeston P, Ravindran P, Kjekshus A and Fjellvåg H 2002 *Phys. Rev. Lett.* **89** 175506
[16] Vajeeston P, Ravindran P, Vidya R, Fjellvåg H and Kjekshus A 2003 *Phys. Rev.* B **68** 212101
[17] Vajeeston P, Ravindran P, Vidya R, Fjellvåg H and Kjekshus A 2003 *Appl. Phys. Lett.* **82** 2257
[18] Araújo C M, Ahuja R, Talyzin A V and Sundqvist B 2005 *Phys. Rev.* B **72** 054125
[19] Vohra Y K and Spencer P T 2001 *Phys. Rev. Lett.* **86** 3068
[20] Bastide J P, Bonnetot B, Letoffe J M and Claudy P 1980 *Mater. Res. Bull.* **15** 1215
[21] Talyzin A V and Sundqvist B 2004 *Phys. Rev.* B **70** 180101
[22] Anderson A M K and Carlson S 2001 *Acta Crystallogr.* B **57** 20

[23] Jordan T H, Dickens B, Schroeder L W and Brown W E 1975 *Acta Crystallogr.* B **31** 669
[24] Auray M, Quarton M and Leblanc M 1995 *Acta Crystallogr.* C **51** 2210
[25] Einarsrud M A, Justnes H, Rytter E and Oye H A 1987 *Polyhedron* **6** 975
[26] Kitajima N, Shimanouchi H, Ono Y and Sasada Y 1982 *Bull. Chem. Soc. Japan.* **55** 2064
[27] Segall M D, Lindan P L D, Probert M J, Pickard C J, Hasnip P J, Clark S J and Payne M C 2002 *J. Phys.: Condens. Matter* **14** 2717
[28] Vanderbilt D 1990 *Phys. Rev.* B **41** 7892
[29] Perdew J P, Chevary J A, Vosko S H, Jackson K A, Pederson M R, Singh D J and Fiolhais C 1992 *Phys. Rev.* B **46** 6671
[30] Fischer T H and Almlof J 1992 *J. Phys. Chem.* **96** 9768
[31] Kresse G and Furthmuller J 1996 *Phys. Rev.* B **54** 11169
[32] Vinet P, Rose J H, Ferrante J and Smith J R 1989 *J. Phys.: Condens. Matter* **1** 1941
[33] Løvvik O M 2005 *Phys. Rev.* B **71** 144111
[34] Setoyama D, Matsunaga J, Muta H, Uno M and Yamanaka S 2004 *J. Alloys Compounds* **381** 215
[35] Tatsumi K, Tanaka I, Tanaka K, Inui H, Yamaguchi M, Adachi H and Mizuno M 2003 *J. Phys.: Condens. Matter* **15** 6549
[36] Jorgensen J D, Hu Z, Teslic S, Argyriou D N and Short S 1999 *Phys. Rev.* B **59** 215
[37] Carlson S and Andersen A M K 2000 *Phys. Rev.* B **61** 11209
[38] Segall M D, Pickard C J, Shah R and Payne M C 1996 *Mol. Phys.* **89** 571
[39] Mulliken R S 1955 *J. Chem. Phys.* **23** 1833
[40] Huang R Z, Wang Y M, Wang J Y and Zhou Y C 2004 *Acta Mater.* **52** 3499
[41] Zhang R J, Wang Y M, Chen D M, Yang Y and Yang K 2006 *Acta Mater.* **54** 465
[42] Rao C N R and Rao K J (ed) 1978 *Phase Transitions in Solids—an Approach to the Study of the Chemistry and Physics of Solids* (New York: McGraw-Hill)